Refractory, Ceramic, and Composite Materials
Тугоплавкие, керамические и композиционные материалы

UDC 666-492.2: 620.193: 549.6
https://doi.org/10.17073/1997-308X-2025-4-50-59

Research article
Научная статья

Effect of ZrO_2–Y_2O_3 powder morphology on CMAS resistance of thermal barrier coatings

S. A. Oglezneva ✉, V. B. Kulmetyeva, A. A. Smetkin, A. E. Malyshev

Perm National Research Polytechnic University
29 Komsomolskiy Prosp., Perm 614990, Russia

✉ svetlana.iron@yandex.ru

Abstract. Corrosion of thermal barrier coatings on gas turbine engine components made of heat-resistant alloys, caused by interaction with molten silicate deposits (CMAS), reduces their high-temperature stability and leads to premature failure during service. The problem of CMAS resistance in coatings with an outer ceramic layer of yttria-stabilized zirconia (YSZ) remains highly relevant, and its solution has important practical implications. The present study focused on zirconia-based ceramic materials used for the deposition of thermal barrier coatings. The interaction of ceramic coatings with silicate deposits was investigated at temperatures up to 1300 °C. Scanning electron microscopy, energy-dispersive spectroscopy, thermogravimetric/differential thermal analysis, and *X*-ray diffraction were employed to study the interaction of CMAS with YSZ on model samples prepared from powders of grades Z7Y10-80A, Zr7Y20-60, and Metco 204NS with different morphologies. The interaction mechanism between CMAS and YSZ at 1200–1300 °C was established. It was shown that the nature and intensity of the interaction strongly depend on the structure and morphology of the ceramic particles. The dense particle structure of ceramics based on Z7Y10-80A and Metco 204NS powders reduces CMAS penetration, in contrast to Zr7Y20-60 powders with a more porous particle structure. The interaction mechanism between CMAS and YSZ was found to be the same for all ceramics studied and occurs through dissolution–precipitation of zirconia in the glass melt. It was demonstrated that with increasing temperature, the degree of zirconia tetragonality changes due to the reduction of yttrium content caused by its diffusion into the glass. This can lead to a polymorphic transformation of zirconia accompanied by volume expansion, followed by cracking and spallation of the thermal barrier coating.

Keywords: gas turbine engine, thermal barrier coatings, ceramic layer, zirconia, silicate deposits, powder morphology

For citation: Oglezneva S.A., Kulmetyeva V.B., Smetkin A.A., Malyshev A.E. Effect of ZrO_2–Y_2O_3 powder morphology on CMAS resistance of thermal barrier coatings. *Powder Metallurgy and Functional Coatings*. 2025;19(4):50–59.
https://doi.org/10.17073/1997-308X-2025-4-50-59

Влияние морфологии керамических порошков ZrO_2–Y_2O_3, используемых в теплозащитных покрытиях, на стойкость к силикатным отложениям

С. А. Оглезнева, В. Б. Кульметьева, А. А. Сметкин, А. Е. Малышев

Пермский национальный исследовательский политехнический университет
Россия, 614990, г. Пермь, Комсомольский пр-т, 29

svetlana.iron@yandex.ru

Аннотация. Коррозия теплозащитных покрытий деталей газотурбинных двигателей, выполненных из жаропрочных сплавов, обусловленная взаимодействием с расплавленными силикатными отложениями (CMAS), снижает их устойчивость к высоким температурам и приводит к преждевременным отказам в эксплуатации. Проблема стойкости к CMAS покрытий с внешним керамическим слоем из диоксида циркония, стабилизированного иттрием, остается весьма актуальной, и ее решение имеет важное практическое применение. Объектом изучения в настоящей работе являлись керамические материалы на основе диоксида циркония, используемые для нанесения теплозащитных покрытий. Исследовано взаимодействие керамических покрытий с силикатными отложениями при температурах до 1300 °С. С помощью сканирующей электронной микроскопии, энергодисперсионной спектроскопии, дериватографии и рентгеноструктурного анализа выполнены исследования взаимодействия CMAS с керамикой YSZ на модельных образцах из порошков марок Z7Y10-80A, Zr7Y20-60 и Metco 204NS различной морфологии. Установлен механизм взаимодействия CMAS и YSZ при t = 1200÷1300 °С. Показано, что характер и интенсивность взаимодействия существенно зависят от строения и морфологии частиц керамики. Плотная структура частиц керамики на основе порошков Z7Y10-80A и Metco 204NS снижает проникновение CMAS в отличие от Zr7Y20-60 с более пористой структурой частиц. Установлено, что характер взаимодействия между CMAS и YSZ един для всех исследуемых керамик и происходит по механизму растворения–осаждения оксида циркония в расплаве стекла. Показано, что с ростом температуры происходит изменение степени тетрагональности оксида циркония, обусловленное снижением содержания иттрия из-за его диффузии в стекло. Это может привести к полиморфной трансформации диоксида циркония с увеличением объема, последующим растрескиванием и отслоением теплозащитного покрытия.

Ключевые слова: газотурбинный двигатель, теплозащитные покрытия, керамический слой, оксид циркония, силикатные отложения, морфология порошков

Для цитирования: Оглезнева С.А., Кульметьева В.Б., Сметкин А.А., Малышев А.Е. Влияние морфологии керамических порошков ZrO_2–Y_2O_3, используемых в теплозащитных покрытиях, на стойкость к силикатным отложениям. *Известия вузов. Порошковая металлургия и функциональные покрытия*. 2025;19(4):50–59. https://doi.org/10.17073/1997-308X-2025-4-50-59

Introduction

The efficiency of gas turbine engines (GTEs) is directly related to the gas temperature at the inlet of the high-pressure turbine (HPT), which exceeds 1200 °C [1; 2]. Such high operating temperatures impose stringent requirements on the protection of components made of heat-resistant alloys used in GTEs. Thermal barrier coatings (TBCs), applied to turbine blades and vanes as well as combustion chamber components, reduce the temperature by approximately 100 °C [3–6].

Modern TBCs consist of an outer ceramic layer and an intermediate metallic bond coat based on nickel superalloys. The outer ceramic layer must combine a range of high-temperature properties, including low thermal conductivity in the operating temperature range, high resistance to thermal shock, phase and structural stability, a high coefficient of thermal expansion, and strong adhesion to the bond coat [7–10]. In current aerospace engine manufacturing, yttria-stabilized zirconia (YSZ) is employed as the outer ceramic layer. This material exhibits low thermal conductivity (2.3 W/(m^2·K) at 1000 °C) for a dense ceramic, a high melting point (2680 °C), and a favorable coefficient of thermal expansion ($11 \cdot 10^{-6}$ K^{-1} at ~1000 °C) [5; 11].

It should be noted that YSZ coatings are susceptible to failures, which are classified as internal and external. Internal failures include defect formation due to phase transformation or excessive temperature gradients during sintering [12]. External failures are usually associated with TBC damage caused by erosion from small (<75 μm) solid particles in the environment or from foreign object damage. Such fine particles typically enter GTEs from dust storms, volcanic ash, and airport runways, where their concentration is relatively high and generally ranges from 350 to 13,000 μg/m^3 [13].

These particles penetrate into the low-pressure compressor and eventually reach the combustion chamber. Under high operating temperatures, they melt, decompose, and deposit on component surfaces, leading to structural degradation and chemical alteration of the TBC. The particles mainly consist of CaO–MgO–Al_2O_3–SiO_2 compounds (*Calcium–Magnesium–Alumina–Silicate – CMAS*). Their detrimental effects on aircraft engine components are well established. Therefore, further research is required to better understand the mechanisms of CMAS interaction with HPT blade coatings [14–16].

Deposition of ceramic top coats for TBCs is carried out using electron-beam physical vapor deposition (EB-PVD) and atmospheric plasma spraying (APS). APS has become the primary method for applying multilayer TBCs due to its high deposition rate, a wide range of adjustable process parameters, relative cost-effectiveness, and suitability for a broad spectrum of powder feedstocks [17–21]. By injecting powders into the plasma jet with a carrier gas, the porosity of the resulting TBC can be controlled. APS technology thus provides flexibility in tailoring the microstructure, particularly of ceramic coatings. The most common microstructure is lamellar, containing microcracks and about 15 % porosity [5; 8].

Coatings produced by APS can develop either porous microstructures or dense ones with vertical cracks. The properties of the feedstock powders play a decisive role in achieving effective TBCs. Typically, the particle size of APS powders ranges from 10 to 100 μm. Oversized particles often fail to melt completely, while undersized ones may bypass the plasma jet and remain in cooler regions, leading to insufficient heating during spraying.

Powder morphology has a strong influence on both processing behavior and in flight dynamics in the plasma jet. To tailor coating properties and functionality, ceramic powders are prepared using methods such as melt crushing, agglomeration–sintering, and agglomeration–spheroidization. These processes produce powders with distinct morphologies: fractured, spherical, or hollow spherical [22–25].

The role of powder morphology in determining resistance to CMAS corrosion has not been adequately investigated and remains a critical issue. The present work therefore aimed to examine the structural and phase evolution of powders with different morphologies, used for TBC deposition, under high temperature exposure to CaO–MgO–Al_2O_3–SiO_2 glass melts. The findings provide insight into the mechanisms of phase evolution in stabilized zirconia powders and lay the groundwork for further studies on full thermal barrier coating systems.

Materials and methods

As starting materials, we used thermal barrier ceramic powders based on yttria stabilized zirconia (YSZ):

– Z7Y10-80A (T: SP LLC, Russia) – agglomerated, sintered, and crushed powder with fractured morphology;

– Zr7Y20-60 (T SFERA LLC, Russia) – agglomerated and sintered powder with spheroidal morphology;

– Metco 204NS (Oerlikon Metco, USA) – agglomerated, plasma treated (HOSP) powder with hollow spherical morphology.

The particle size distribution of the YSZ powders was determined by laser diffraction (Analizette 22 NanoTech, Fritsch, Germany) and is summarized in Table 1.

For CMAS investigations, a model glass was prepared. According to *X*-ray fluorescence analysis (EDX 800HS spectrometer, Shimadzu, Japan), its composition was (wt. %): SiO_2 – 53.3, CaO – 30.4, Al_2O_3 – 10.7, MgO – 5.4. The glass was first ground in a jasper mortar and then milled in a planetary ball mill in water for 2 h at a rotation speed of 160 rpm. The dried powder was sieved. Its chemical composition closely matched the CMAS glass reported in the literature [26–28], which represents the average composition of deposits found on turbine blades in service (SiO_2 – 48.5, CaO – 33.2, Al_2O_3 – 11.8, MgO – 6.5 wt. %). Simultaneous thermal analysis (ZCT H, Jing Yi Gao Ke) showed that melting started at 1200 °C and reached its maximum at 1244 °C.

Table 1. **Particle size distribution of YSZ ceramic powders**

Таблица 1. **Гранулометрический состав керамических порошков YSZ**

Powder grade	Production method	Particle size distribution, μm		
		d_{10}	d_{50}	d_{90}
Z7Y10-80A	Sintering, crushing	4.0	48.9	75.3
Zr7Y20-60	Agglomeration-sintering	11.2	28.1	37.9
Metco 204NS	Agglomeration, plasma treatment (HOSP)	13.4	41.9	62.8

Model samples for studying CMAS infiltration and microstructural evolution were fabricated by pressing YSZ powders followed by sintering. For binder preparation, a 4% polyvinyl alcohol solution (GOST 10779-78) was added in an amount corresponding to 10 wt. % of the powder. Pressing was performed on a manual hydraulic press (Carl Zeiss, Germany) under a specific pressure of 1.5 t/cm^2. Sintering was carried out in a HT 64/17 furnace (Nabertherm, Germany) at 1700 °C for 2 h.

On the surface of the sintered samples (Z7Y10-80A, Zr7Y20-60, and Metco 204NS), a suspension of CMAS powder in ethanol was applied at a loading of 20 mg/cm^2. High temperature tests of the samples with surface applied suspensions were performed in air in the HT 64/17 electric furnace. The heating rate was 10 °C/min, and the exposure temperature ranged from 1200–1300 °C with holding times ranging from 2 to 24 h.

To analyze high temperature chemical reactions between YSZ and CMAS in more detail, powder mixtures were prepared at a 3:1 ratio. The mixtures were homogenized in ethanol, dried, and pressed into pellets at 50 MPa, followed by isothermal treatment at 1200–1300 °C for 2 h.

Microstructural analysis of cross sections was performed using a scanning electron microscope (SEM EM 30AX, Coxem Co. Ltd., Republic of Korea) equipped with an energy dispersive spectrometer (EDS). Phase composition and structural parameters were determined on an *X*-ray diffractometer (XRD 6000, Shimadzu, Japan) using full profile analysis. Diffraction patterns were recorded over a 2θ range of 20–90° with CuK_α radiation, a step size of 0.02°, and a counting time of 2 s per step. Qualitative phase analysis was carried out using the Crystallographica Search Match (CSM) program and the PDF database of the International Centre for Diffraction Data (ICDD).

Results and discussion

Structure of YSZ ceramic powders

Analysis of the particle size distribution (Table 1) showed that the average particle sizes of powders Z7Y10-80A and Metco 204NS are comparable, with d_{50} values of 48.9 and 41.9 μm, respectively. However, Z7Y10-80A contains the largest fraction of fine particles compared with the other powders. The smallest average particle size, d_{50} = 28.1 μm, was observed for Zr7Y20-60.

SEM images of powder morphology and cross-sections are presented in Fig. 1. Based on morphometric parameters, Z7Y10-80A exhibits a fractured morphology, Zr7Y20-60 is nearly spherical, and Metco 204NS is predominantly hollow spherical. Particles of all powders, except Metco 204NS, are porous throughout their volume. Metco 204NS contains both hollow spherical particles and non hollow porous particles similar in structure to the other powders. The shells of the hollow spheres are notably denser compared to the non hollow particles.

XRD analysis (Fig. 2) showed that the Z7Y10-80A and Zr7Y20-60 powders are composed of tetragonal ZrO_2 (space group $P4_2/nmc$, No. 137). The results of Rietveld full-profile refinement of the structural parameters and phase composition are presented in Table 2. The lattice parameters of the tetragonal phase are nearly identical to the reference values (PDF card No. 80-2155). The Metco 204NS powder consists of tetragonal ($P4_2/nmc$, No. 137) and monoclinic ZrO_2 ($P2_1/c$, No. 14) in proportions of 79 and 21 %, respec-

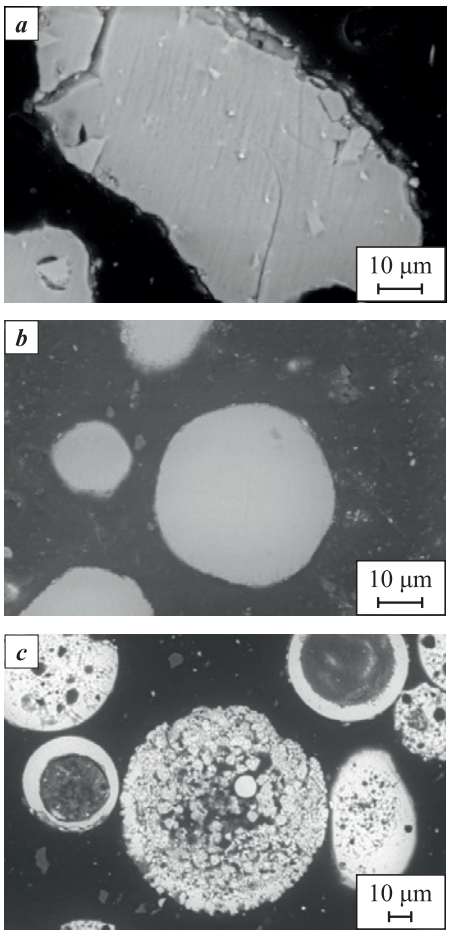

Fig. 1. SEM images of the morphology and cross sections of YSZ ceramic powder particles
Z7Y10-80A (***a***), Zr7Y20-60 (***b***) and Metco 204NS (***c***)

Рис. 1. СЭМ-изображения морфологии и поперечных сечений частиц керамических порошков
Z7Y10-80A (***a***), Zr7Y20-60 (***b***) и Metco 204NS (***c***)

Table 2. **Structural parameters of YSZ powders**

Таблица 2. **Структурные параметры порошков YSZ**

Powder grade	Phase	Lattice parameters, nm			Crystallite size *D*, nm	Lattice microstrain *da*/*a*, %
		a	*b*	*c*		
Z7Y10-80A	*t*	0.36142	0.36142	0.51706	21	0.14
Zr7Y20-60	*t*	0.36131	0.36131	0.51670	51	0.06
Metco 204NS	*t*	0.36143	0.36143	0.51580	200	0.01
	m	0.51617	0.52052	0.53221	65	0.05

tively. The smallest crystallite size was observed for Z7Y10-80A, while the largest was for Metco 204NS. The evaluation of lattice microstrain *da*/*a* indicated the highest distortions in Z7Y10-80A, which can be attributed to mechanical crushing.

XRD analysis of the model samples sintered at 1700 °C for 2 h showed that their phase composition did not differ from that of the as received powders.

The mechanism of interaction between YSZ ceramics and CMAS has been widely investigated and described in numerous studies [13; 15; 26; 27; 29–31]. In general, YSZ dissolves into the CMAS melt, followed by the reprecipitation of ZrO_2 grains in various polymorphic forms and compositions, depending on the local melt chemistry. Since Y^{3+} ions have much higher solubility in CMAS than Zr^{4+} ions, they readily diffuse into the melt, leading to zirconia depletion. This depletion facilitates the phase transformation of YSZ from tetragonal to monoclinic.

Interaction of Z7Y10 80A with CMAS

The interaction of CMAS with ceramic powders begins at temperatures below the melting point of the glass due to the formation of a eutectic in the SiO_2–CaO–Al_2O_3 system [29; 32]. As a result, regardless of particle morphology, interaction with CMAS is already observed at 1200 °C.

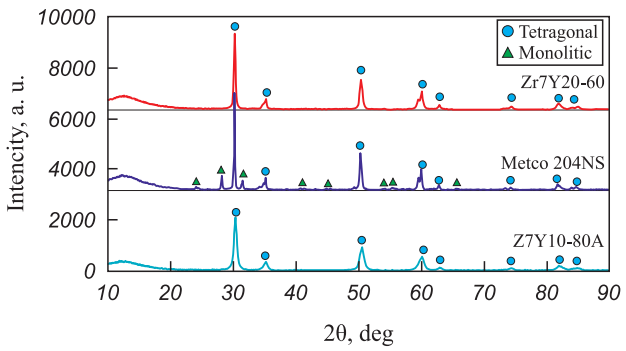

Fig. 2. XRD patterns of YSZ powders

Рис. 2. Дифрактограммы исходных порошков YSZ

As shown above, the particles of the Z7Y10-80A powder (Fig. 1, *a*) possess a dense structure determined by the production method, which strongly influences their interaction with CMAS. At 1200 °C, interaction is confined to a near-surface layer up to ~2 μm thick, while the dense particle structure remains largely intact (Fig. 3, *a*). When the temperature is raised to 1300 °C, dissolution/precipitation processes in YSZ are activated, resulting in loosening of the particle structure (Fig. 3, *b*). The glass melt penetrates from the interparticle space into the particle interior, causing the particle boundaries to blur.

Since the sensitivity of XRD to detect subtle phase composition changes during CMAS interaction is relatively low when glass is simply applied to the surface of Z7Y10-80A, additional mixed samples with a Z7Y10-80A:CMAS ratio of 3:1 were prepared. These were heated in air at 1200, 1250, and 1300 °C for 2 h. This approach enabled a more precise analysis of the CMAS–ceramic interaction mechanisms.

Fig. 4 shows the XRD patterns of the Z7Y10-80A:CMAS samples after exposure to these temperatures. The incorporation of 6–8 wt. % Y_2O_3 into ZrO_2 results in the formation of a metastable tetragonal *t*′-phase (the so called non transformable phase), in contrast to the less stable tetragonal *t*-phase. To distinguish between the two tetragonal modifications (*t* and *t*′), the $c/a\sqrt{2}$ ratio – reflecting the degree of tetragonality – is used. For the *t*′-phase, this ratio approaches 1.010 [33].

The as received Z7Y10-80A powder consists of tetragonal zirconia, with no characteristic doublets observed at $2\theta \approx 35°$ and 60°. After testing, the XRD patterns clearly show peak splitting at these angles, along with the emergence of the cubic (400) reflection in the 2θ range of 72–76°. In the as received powder, the degree of tetragonality was 1.0116 and remained unchanged after exposure at 1200 °C. Raising the temperature to 1250 °C led to an increase in tetragonality, associated with yttrium depletion in YSZ, i.e., the decomposition of the *t*-phase into *t*- and *c*-phases.

At 1300 °C, counter diffusion of Ca and Mg from the glass into YSZ causes a reduction in tetragonality,

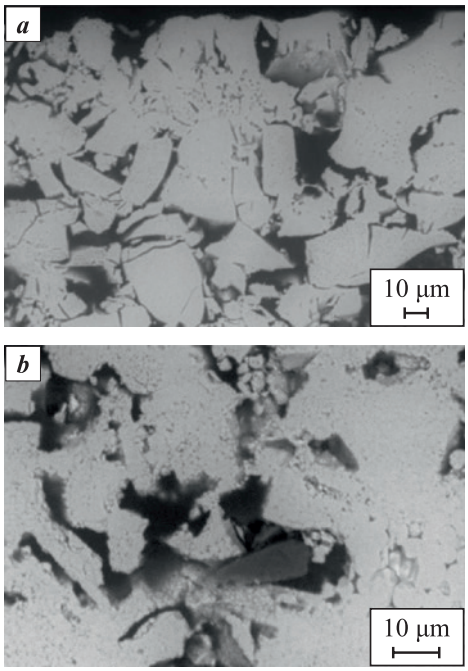

Fig. 3. SEM images of Z7Y10-80A samples after interaction with CMAS at 1200 °C for 2 h (***a***) and 1300 °C for 12 h (***b***)

Рис. 3. СЭМ-изображения образцов Z7Y10-80A после взаимодействия с CMAS при t = 1200 °C, τ = 2 ч (***a***), t = 1300 °C, τ = 12 ч (***b***)

although it does not return to its original value (Table 3). The variation in tetragonality as a function of yttrium content is consistent with the findings reported in [34], where it was shown that, irrespective of the synthesis method, the tetragonal character of YSZ powders diminishes with increasing yttrium content.

Table 3. **Lattice parameters of the tetragonal phase in YSZ**

Таблица 3. **Параметры кристаллической решетки тетрагональной фазы YSZ**

Powder grade	t, °C	a, nm	c, nm	$c/a\sqrt{2}$
Z7Y10-80A	20	0.36142	0.51706	1.0116
	1200	0.36145	0.51707	1.0115
	1250	0.36087	0.51710	1.0132
	1300	0.36104	0.51692	1.0124
Zr7Y20-60	20	0.36131	0.51670	1.0112
	1200	0.36091	0.51661	1.0122
	1250	0.36094	0.51659	1.0120
	1300	0.36041	0.51701	1.0143
Metco 204NS	20	0.36143	0.51580	1.0091
	1200	0.36135	0.51663	1.0110
	1250	0.36150	0.51724	1.0117
	1300	0.36179	0.51767	1.0118

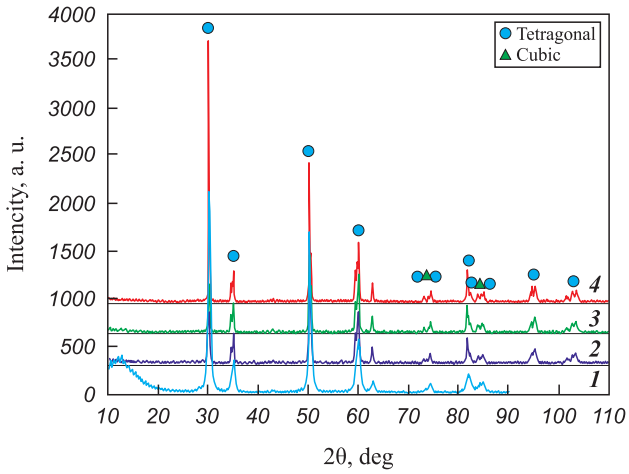

Fig. 4. XRD patterns of Z7Y10-80A samples after interaction with CMAS at different temperatures

1 – as-received, ***2*** – 1200 °C, ***3*** – 1250 °C, ***4*** – 1300 °C

Рис. 4. Дифрактограммы образцов Z7Y10-80A после взаимодействия с CMAS при различных температурах

1 – исходный, ***2*** – 1200 °C, ***3*** – 1250 °C, ***4*** – 1300 °C

Interaction of Zr7Y20-60 with CMAS

The Zr7Y20-60 ceramic particles have a porous surface surrounding a dense core (Fig. 1, *b*). This morphology makes them prone to CMAS melt infiltration, not only into the macropores but also deeper into the particle volume. Interaction between YSZ and CMAS is already evident at 1200 °C (Fig. 5), and at 1300 °C it becomes more pronounced, with the boundaries between individual ceramic grains disappearing and an extensive reaction zone forming.

The as received Zr7Y20-60 powder consists of tetragonal zirconia; however, the characteristic doublets are already distinguishable at $2\theta \approx 35°$ and 60° (Fig. 6). After exposure at 1200 °C, these doublets become clearly resolved. As the temperature increases, the degree of tetragonality rises from 1.0112 to 1.0143 (Table 3). At 1300 °C, the emergence of the cubic phase is indicated by the appearance of the (400) peak between the tetragonal (004) and (220) reflections.

Interaction of Metco 204NS with CMAS

The Metco 204NS ceramic powder consists of both hollow spherical particles with a dense shell and non hollow particles with a porous structure. The latter interact most intensively with CMAS due to glass infiltration (Fig. 7). As the temperature increases to 1300 °C, the boundaries between individual non hollow particles gradually disappear, leading to the formation of an extensive reaction zone. In contrast, the dense

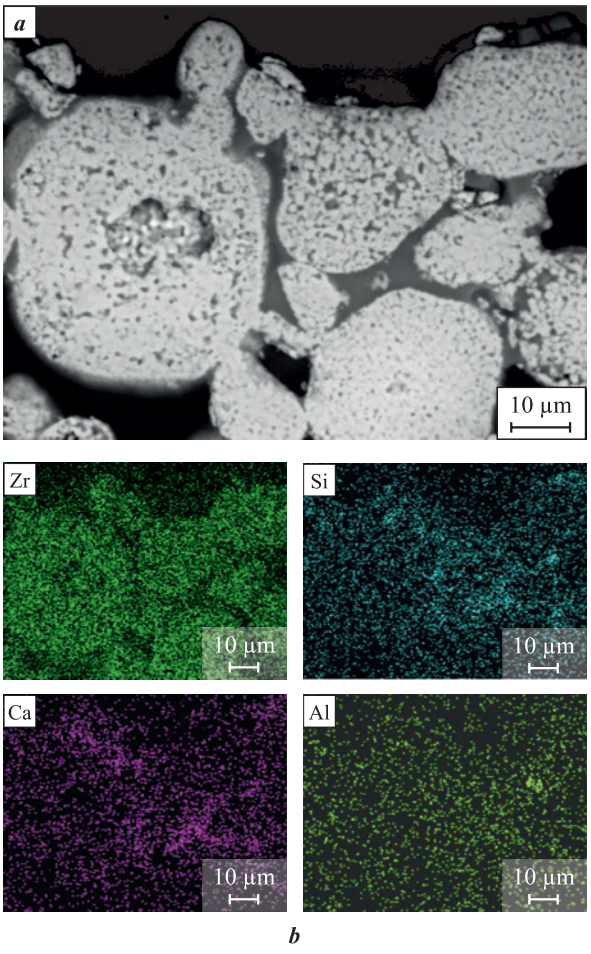

Fig. 5. SEM image (***a***) and EDS analysis (***b***) of Zr7Y20-60 samples after interaction with CMAS at 1200 °C for 2 h

Рис. 5. СЭМ-изображение (***a***) и результаты EDS-анализа (***b***) образцов Zr7Y20-60 после взаимодействия с CMAS при t = 1200 °C в течение 2 ч

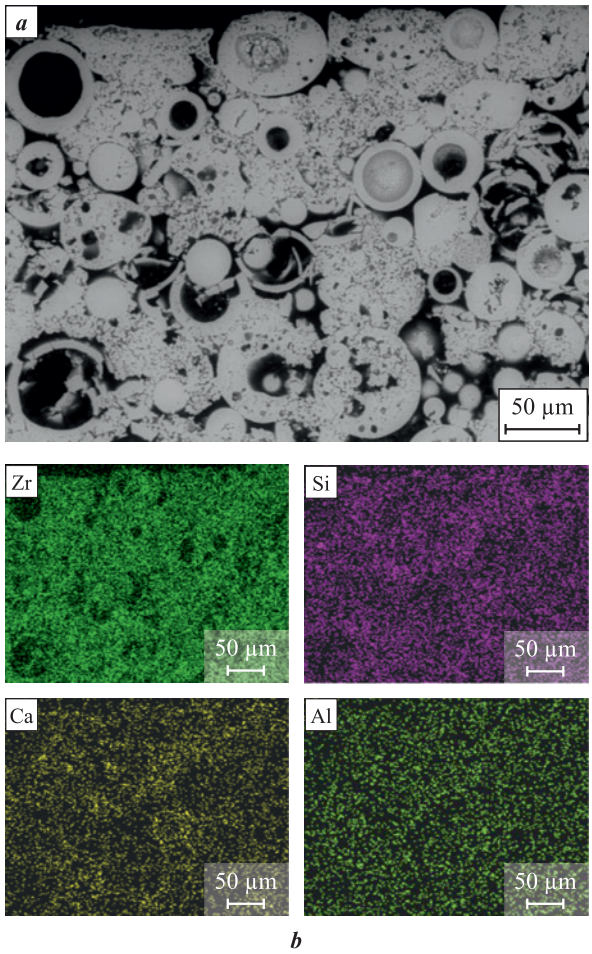

Fig. 7. SEM image (***a***) and EDS analysis (***b***) of Metco 204NS samples after interaction with CMAS at 1300 °C for 24 h

Рис. 7. СЭМ-изображение (***a***) и результаты EDS-анализа (***b***) образцов Metco 204NS после взаимодействия с CMAS при t = 1300 °C в течение 24 ч

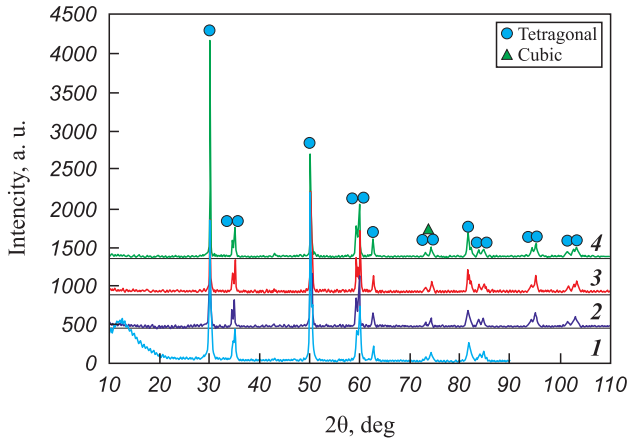

Fig. 6. XRD patterns of Zr7Y20-60 samples after interaction with CMAS at different temperatures

1 – as-received, ***2*** – 1200 °C, ***3*** – 1250 °C, ***4*** – 1300 °C

Рис. 6. Дифрактограммы образцов Zr7Y20-60 после взаимодействия с CMAS при различных температурах

1 – исходный, ***2*** – 1200 °C, ***3*** – 1250 °C, ***4*** – 1300 °C

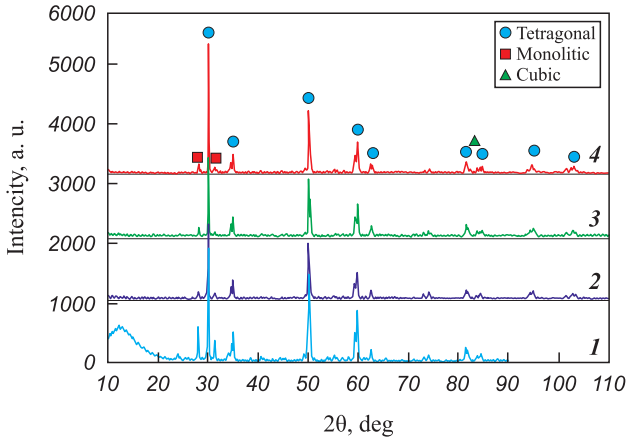

Fig. 8. XRD patterns of Metco 204NS samples after interaction with CMAS at different temperatures

1 – as-received, ***2*** – 1200 °C, ***3*** – 1250 °C, ***4*** – 1300 °C

Рис. 8. Дифрактограммы образцов Metco 204NS после взаимодействия с CMAS при различных температурах

1 – исходный, ***2*** – 1200 °C, ***3*** – 1250 °C, ***4*** – 1300 °C

shells of the spherical particles remain the most resistant to CMAS attack up to 1300 °C, preserving their structural integrity.

XRD analysis revealed that after CMAS corrosion testing the monoclinic phase fraction (m-ZrO_2) decreased from 20.6 to 10.0 % (Fig. 8). This was accompanied by a reduction in the intensity of the ($\bar{1}11$) and (111) reflections and an increase in the degree of tetragonality (see Table 2). These changes are attributed to additional stabilization of zirconia by calcium and magnesium oxides. At 1300 °C, the cubic (400) reflection was also detected.

Conclusion

The study of CMAS interaction with TBC ceramics based on Z7Y10-80A, Zr7Y20-60, and Metco 204NS powders using model samples has demonstrated that the interaction mechanism between CMAS and YSZ is the same for all yttria containing ceramics. It is governed by the dissolution–precipitation of zirconia in the glass melt. Exposure to CMAS at 1200–1300 °C leads to the formation of a new yttria depleted tetragonal zirconia phase as a result of yttrium diffusion into the glass. With increasing temperature, the degree of tetragonality changes due to further yttrium depletion. However, the counter diffusion of Ca and Mg ions from the glass into zirconia is insufficient to restore the initial tetragonality values. As a result, zirconia may undergo polymorphic transformation accompanied by volume expansion, cracking, and eventual spallation of the TBC.

The extent and character of CMAS–YSZ interaction were shown to depend strongly on the structure and morphology of the ceramic particles. A dense particle structure, as in ceramics produced from Z7Y10-80A and Metco 204NS powders, reduces CMAS infiltration, whereas the more porous structure of Zr7Y20-60 particles promotes deeper penetration and more extensive interaction.

References / Список литературы

1. Kablov E.N. Cast blades of gas turbine engines: Alloys, technologies, coatings. 2nd ed. Moscow: Nauka, 2006. 632 p. (In Russ.).

   Каблов Е.Н. Литые лопатки газотурбинных двигателей: Сплавы, технология, покрытия. 2-е изд. М.: Наука, 2006. 632 с.
2. Zeraati M., Oganov A., Fan T., Solodovnikov S. Searching for low thermal conductivity materials for thermal barrier coatings: A theoretical approach. *Physical Review Materials*. 2024;8(3):033601. https://doi.org/10.1103/PhysRevMaterials.8.033601
3. Huang L.L., Meng H.M., Tang J., Li S., Yu Z.Q. Overview on double ceramic layer thermal barrier coatings. *Advanced Materials Research*. 2014;1053:364–372. https://doi.org/10.4028/www.scientific.net/amr.1053.364
4. Liu B., Liu Y., Zhu C., Xiang H., Chen H., Sun L., Gao Y., Zhou Y. Advances on strategies for searching for next generation thermal barrier coating materials. *Journal of Materials Science and Technology*. 2019;35(5):833–851. https://doi.org/10.1016/j.jmst.2018.11.016
5. Vaßen R., Bakan E., Mack D.E., Guillon O.A Perspective on thermally sprayed thermal barrier coatings: current status and trends. *Journal of Thermal Spray Technology*. 2022;31(4):685–698. https://doi.org/10.1007/s11666-022-01330-2
6. Pankov V.P., Babayan A.L., Kulikov M.V., Kossoy V.A., Varlamov B.S. Heat-protective coatings for turbine blades of aircraft gas turbine engines. *Polzunovskiy vestnik*. 2021;1:161–172. (In Russ.). https://doi.org/10.25712/ASTU.2072-8921.2021.01.023

   Панков В.П., Бабаян А.Л., Куликов М.В., Коссой В.А., Варламов Б.С. Теплозащитные покрытия лопаток турбин авиационных газотурбинных двигателей. *Ползуновский Вестник*. 2021;1:161–172. https://doi.org/10.25712/ASTU.2072-8921.2021.01.023
7. Dudnik E., Lakiza S., Hrechanyuk I., Ruban A.K., Redko V.P., Marek I.O., Shmibelsky V.B., Makudera A.A., Hrechanyuk N.I. Thermal barrier coatings based on ZrO_2 solid solutions. *Powder Metallurgy and Metal Ceramics*. 2020;59(3):179–200. https://doi.org/10.1007/s11106-020-00151-8
8. Bakan E., Vaßen R. Ceramic top coats of plasma-sprayed thermal barrier coatings: materials, processes, and properties. *Journal of Thermal Spray Technology*. 2017;26(12): 992–1010. https://doi.org/10.1007/s11666-017-0597-7
9. Sezavar A., Sajjadi S.A. A review on the performance and lifetime improvement of thermal barrier coatings. *Journal of the European Ceramic Society*. 2025;45(1):117274. https://doi.org/10.1016/j.jeurceramsoc.2025.117274
10. Iqbal A., Moskal G., Cavaleiro A., Amjad A., Khan M.J. The current advancement of zirconate based dual phase system in thermal barrier coatings (TBCs): New modes of the failures: Understanding and investigations. *Alexandria Engineering Journal*. 2024;91:161–196. https://doi.org/10.1016/j.aej.2024.01.063
11. Bogdan M., Peter I. A comprehensive understanding of thermal barrier coatings (TBCs): applications, materials, coating design and failure mechanisms. *Metals*. 2024;14(5):575. https://doi.org/10.3390/met14050575
12. Pakseresht A., Sharifianjazi F., Esmaeilkhanian A., Bazli L., Reisi Nafchi M., Bazli M., Kirubaharan K. Failure mechanisms and structure tailoring of YSZ and new candidates for thermal barrier coatings: A systematic review. *Materials and Design*. 2022;222:111044. https://doi.org/10.1016/j.matdes.2022.111044
13. Nieto A., Agrawal R., Bravo L., Hofmeister-Mock C., Pepi M., Ghoshal A. Calcia–magnesia–alumina–silicate (CMAS) attack mechanisms and roadmap towards Sandphobic thermal and environmental barrier coatings. *Inter-*

national Materials Reviews. 2021;66(7):451–492. https://doi.org/10.1080/09506608.2020.1824414

14. Guo L., Xin H., Li Y., Yu Y. Self-crystallization characteristics of calcium-magnesium-alumina-silicate (CMAS) glass under simulated conditions for thermal barrier coating applications. *Journal of the European Ceramic Society*. 2020;40(15):5683–5691. https://doi.org/10.1016/j.jeurceramsoc.2020.07.025
15. Tolmachev Ya.V., Zavarzin S.V., Loshchinina A.O., Knyazev A.V. High temperature oxide corrosion of ceramic materials in turbine engines. *Trudy VIAM*. 2023;7:69–83. (In Russ.). https://doi.org/10.18577/2307-6046-2023-0-7-69-83

    Толмачев Я.В., Заварзин С.В., Лощинина А.О., Князев А.В. Высокотемпературная оксидная коррозия керамических материалов ГТД. *Труды ВИАМ*. 2023;7:69–83. https://doi.org/10.18577/2307-6046-2023-0-7-69-83
16. Nair R.B., Brabazon D. Calcia magnesia alumino silicate (CMAS) corrosion attack on thermally sprayed thermal barrier coatings: A comprehensive review. *npj Materials Degradation*. 2024;8:44. https://doi.org/10.1038/s41529-024-00462-w
17. Kadam N.R., Karthikeyan G., Jagtap P.M., Kulkarni D.M. An atmospheric plasma spray and electron beam-physical vapour deposition for thermal barrier coatings: a review. *Australian Journal of Mechanical Engineering*. 2022;21(5):1729–1754. https://doi.org/10.1080/14484846.2022.2030088
18. Vaßen R., Bakan E., Mack D., Guillon O. A perspective on thermally sprayed thermal barrier coatings: current status and trends. *Journal of Thermal Spray Technology*. 2022;31(4):685–698. https://doi.org/10.1007/s11666-022-01330-2
19. Kubaszek T., Goral M., Pedrak P. Influence of air plasma spraying process parameters on the thermal barrier coating deposited with micro- and nanopowders. *Materials Science-Poland*. 2022;40(3):80–92. https://doi.org/10.2478/msp-2022-0034
20. Puzrjakov A.F. Theoretical foundations of plasma spraying technology. Moscow: Publishing House of Bauman Moscow State Technical University, 2003. 360 p. (In Russ.).

    Пузряков А.Ф. Теоретические основы технологии плазменного напыления. М.: Изд. МГТУ им. Н.Э. Баумана, 2003. 360 с.
21. Bernard B.A., Quet A., Bianchi L., Joulia A., Malie A., Schick V., Remy B. Thermal insulation properties of YSZ coatings: suspension plasma spraying (SPS) versus electron beam physical vapor deposition (EB-PVD) and atmospheric plasma spraying (APS). *Surface and Coatings Technology*. 2017;318:122–128. https://doi.org/10.1016/j.surfcoat.2016.06.010
22. Il'inkova T.A., Barsukova E.A., Tagirov A.T. The relationship between the characteristics of powder materials and the mechanical properties of plasma thermal barrier coatings. *Vestnik Kazanskogo tekhnologicheskogo universiteta*. 2015;18(15):116–121.(In Russ.).

    Ильинкова Т.А., Барсукова Е.А., Тагиров А.Т. Взаимосвязь характеристик порошковых материалов и механических свойств плазменных теплозащитных покрытий. *Вестник Казанского технологического университета*. 2015;18(15):116–121.
23. Qiu J., Yu D., Chen Y., Li D., Islam M.S., Peng X. Controllable preparation of YSZ-STHS in arc plasma spheroidization: exploring the plasma flow characteristics' impact on powder quality. *Ceramics International*. 2024;50(15):26569–26582. https://doi.org/10.1016/j.ceramint.2024.04.385
24. Guo H.B., Murakami H., Kuroda S. Effect of hollow spherical powder size distribution on porosity and segmentation cracks in thermal barrier coatings. *Journal of the American Ceramic Society*. 2006;89(12):3797–3804. https://doi.org/10.1111/j.1551-2916.2006.01322.x
25. Zhao L., Zhang Z., Duan Y., Cui H., Gao Y. Preparation of yttria-stabilized zirconia hollow sphere with reduced shell thickness by controlling ambient temperature during plasma process. *Coatings*. 2018;8(7):245. https://doi.org/10.3390/coatings8070245
26. Kraemer S., Yang J., Levi C., Johnson C. Thermomechanical interaction of thermal barrier coatings with molten CaO–MgO–Al_2O_3–SiO_2 (CMAS) Deposits. *Journal of the American Ceramic Society*. 2006;89:3167–3175. https://doi.org/10.1111/j.1551-2916.2006.01209.x
27. Morelli S., Testa V., Bolelli G., Ligabue O., Molinari E., Antolotti N., Lusvarghi L. CMAS corrosion of YSZ thermal barrier coatings obtained by different thermal spray processes. *Journal of the European Ceramic Society*. 2020;40(12):4084–4100. https://doi.org/10.1016/j.jeurceramsoc.2020.04.058
28. Wu Y., Luo H., Cai C., Wang Y., Zhou Y., Yang L., Zhou G. Comparison of CMAS corrosion and sintering induced microstructural characteristics of APS thermal barrier coatings. *Journal of Material Science and Technology*. 2019;35(3):440–447. https://doi.org10.1016/j.jmst.2018.09.046
29. Vidal-Setif M.H., Rio C., Boivin D., Lavigne O. Microstructural characterization of the interaction between 8YPSZ (EB-PVD) thermal barrier coatings and a synthetic CAS. *Surface and Coatings Technology*. 2014;239:41–48. https://doi.org/10.1016/j.surfcoat.2013.11.014
30. Ramachandran C.S., Balasubramanian V., Ananthapadmanabhan P.V. Thermal cycling behaviour of plasma sprayed lanthanum zirconate based coatings under concurrent infiltration by a molten glass concoction. *Ceramics International*. 2013;39(2):1413–1431. https://doi.org/10.1016/j.ceramint.2012.07.084
31. Boissonnet G., Chalk C., Nicholls J., Bonnet G., Pedraza F. Thermal insulation of CMAS (Calcium-Magnesium-Alumino-Silicates)-attacked plasma-sprayed thermal barrier coatings. *Journal of the European Ceramic Society*. 2020;40(5):2042–2049. https://doi.org/10.1016/j.jeurceramsoc.2019.12.040
32. Pratskova S.E., Burmistrov V.A., Starikova A.A. Thermodynamic modeling of oxide melts of CaO–Al_2O_3–SiO_2 systems. *Izvestiya vysshikh uchebnykh zavedeniy. Khimiya i khimicheskaya tekhnologiya*. 2020;63(1):45–50. (In Russ.). https://doi.org/10.6060/ivkkt.20206301.6054

Працкова С.Е., Бурмистров В.А., Старикова А.А. Термодинамическое моделирование оксидных расплавов системы CaO–Al_2O_3–SiO_2. *Известия высших учебных заведений. Химия и химическая технология*. 2020;63(1):45–50.
https://doi.org/10.6060/ivkkt.20206301.6054

33. Tolkachev O.S., Dvilis E.S., Alishin T.R., Khasanov O.L., Miheev D.A., Chzhan T. Assessment of the hydrothermal resistance of Y-TZP ceramics by the degree of tetragonality of major phases. *Pis'ma o materialakh*. 2020;10(4): 416–421. (In Russ.).
https://doi.org/10.22226/2410-3535-2020-4-416-421

Толкачёв О.С., Двилис Э.С., Алишин Т.Р., Хасанов О.Л., Михеев Д.А., Чжан Ц. Оценка гидротермальной стойкости керамики Y-TZP по степени тетрагональности основных фаз. *Письма о материалах*. 2020;10(4):416–421.
https://doi.org/10.22226/2410-3535-2020-4-416-421

34. Viazzi C., Bonino J.-P., Ansart F., Barnabe A. Structural study of metastable tetragonal YSZ powders produced via a sol-gel route. *Journal of Alloys and Compdounds*. 2008;452(2):377–383.
https://doi.org/10.1016/j.jallcom.2006.10.155

Information about the Authors

Svetlana A. Oglezneva – Dr. Sci. (Eng.), Associate Professor of the Department of mechanics of composite materials and structures, Perm National Research Polytechnic University (PNRPU)
ORCID: 0000-0002-5529-4259
E-mail: svetlana.iron@yandex.ru

Valentina B. Kulmetyeva – Cand. Sci. (Eng.), Associate Professor of the Department of mechanics of composite materials and structures, PNRPU
ORCID: 0000-0002-5214-0932
E-mail: kulmetevavb@pstu.ru

Andrey A. Smetkin – Cand. Sci. (Eng.), Associate Professor of the Department of Mechanics of composite materials and structures, PNRPU
ORCID: 0000-0001-8736-0575
E-mail: smetkinaa@pstu.ru

Alexander E. Malyshev – Master's Degree Student at the Advanced Engineering School "Higher School of Aviation Engine Engineering", PNRPU
ORCID: 0009-0004-6923-9316
E-mail: malyschev.4lex@yandex.ru

Сведения об авторах

Светлана Аркадьевна Оглезнева – д.т.н., профессор, доцент кафедры механики композиционных материалов и конструкций, Пермский национальный исследовательский политехнический университет (ПНИПУ)
ORCID: 0000-0002-5529-4259
E-mail: svetlana.iron@yandex.ru

Валентина Борисовна Кульметьева – к.т.н., доцент кафедры механики композиционных материалов и конструкций, ПНИПУ
ORCID: 0000-0002-5214-0932
E-mail: kulmetevavb@pstu.ru

Андрей Алексеевич Сметкин – к.т.н., доцент кафедры механики композиционных материалов и конструкций, ПНИПУ
ORCID: 0000-0001-8736-0575
E-mail: smetkinaa@pstu.ru

Александр Евгеньевич Малышев – студент магистратуры Передовой инженерной школы «Высшая школа авиационного двигателестроения», ПНИПУ
ORCID: 0009-0004-6923-9316
E-mail: malyschev.4lex@yandex.ru

Contribution of the Authors

S. A. Oglezneva – scientific supervision, analysis of research results, manuscript revision, revision of conclusions.
V. B.Kulmetyeva – development of the main concept, formulation of the research aim and objectives, manuscript drafting, analysis of research results, formulation of conclusions.
A. A. Smetkin – experiment preparation, conducting experiments, formulation of the research objectives, manuscript drafting, formulation of conclusions.
A. E. Malyshev – sample testing, manuscript drafting

Вклад авторов

С. А. Оглезнева – научное руководство, анализ результатов исследований, корректировка текста, корректировка выводов.
В. Б. Кульметьева – формирование основной концепции, постановка цели и задачи исследования, подготовка текста, анализ результатов исследований, формулировка выводов.
А. А. Сметкин – подготовка эксперимента, проведение экспериментов, постановка цели и задачи исследования, подготовка текста, формулировка выводов.
А. Е. Малышев – проведение испытаний образцов, подготовка текста статьи.

Received 12.05.2025
Revised 18.06.2025
Accepted 20.06.2025

Статья поступила 12.05.2025 г.
Доработана 18.06.2025 г.
Принята к публикации 20.06.2025 г.